Pergamon

Int. J. Solids Structures Vol. 34, Nos 33–34, pp. 4421–4446, 1997

0020–7683/97 $17.00 + .00

PII: S0020–7683(97)00012–7

DISPERSED-PHASE MARTENSITIC TRANSFORMATION CONTROLLED DEFORMATION BEHAVIOR OF TWO-PHASE METALLIC MATERIALS

M. GRUJICIC and N. SANKARAN
Department of Mechanical Engineering, Clemson University, Clemson, SC 29634, U.S.A.

(*Received* 10 *July* 1996; *in revised form* 21 *November* 1996)

Abstract—A constitutive model which describes transformation plasticity accompanying stress-assisted martensitic transformation in two-phase material systems consisting of a stable matrix and a transforming dispersed phase is developed. The model consists of two parts: (a) a transformation thermodynamics/kinetics law describing the evolution of the transformed fraction of dispersed particles and (b) a constitutive law describing plastic flow resistance of the evolving three-phase (matrix phase, dispersed parent phase, dispersed product phase) composite material. The model is constructed in such a way that it can be readily implemented in a finite element program suitable for the analysis of boundary value problems. The model is used to analyze the uniaxial tensile behavior of the two-phase gamma Ti-Al matrix/beta (Ti-Al-V-Fe) phase system in order to rationalize an experimentally observed nearly 100% increase in tensile ductility of the material due to the martensitic transformation in the beta phase. The model is also used to study the uniaxial tensile behavior of beta/alpha two phase Ti-10V-2Fe-3Al (wt.%) alloy characterized by a sigmoidal stress–strain curve. A reasonably good agreement is obtained between the model predictions and the experimental data. © 1997 Elsevier Science Ltd.

INTRODUCTION

During the last two decades, it has been unequivocally established that stress induced martensitic transformations can significantly enhance the tensile ductility and the fracture toughness of high-strength, brittle materials. The effect of martensitic transformation has been most extensively investigated and major improvements in materials tensile ductility and fracture toughness achieved in ZrO_2 and in various ceramics containing ZrO_2 second phase particles, e.g. Evans and Cannon (1986), and in ultra-high strength secondary hardening steels, Olson (1987). In our recent study, Grujicic and Dang (1996), we found that adding to the gamma TiAl intermetallic 10 vol.% of a metastable Ti-26Al-52V-5Fe (wt.%) b.c.c. beta phase which undergoes a stress-induced martensitic transformation gives rise to a nearly 100% increase in the tensile ductility and the fracture toughness of the otherwise single phase gamma TiAl.

The fundamental basis for comprehending the phenomenon of martensitic transformation-enhanced ductility and toughness resides in the thermodynamics and associated kinetics of the stress-assisted transformation. The basic thermodynamics along with consideration of the pertinent martensitic nucleation and growth processes, permits description of the stress–strain characteristics of materials containing various types of transforming particles. The ensuing trends in stress–strain behavior allow material constitutive laws to be determined which, in turn, lead directly to description of the (crack tip) stress and displacement fields and to the assessment of the resultant transformation enhanced ductility and toughness.

A materials constitutive model which takes into account the basic thermodynamic and kinetic aspects of deformation-induced martensitic transformation in metastable steels has recently been developed by Stringfellow *et al.* (1992). This model cannot be used to analyze the observed transformation-enhanced ductility and toughness effects in the gamma TiAl-based system discussed earlier for two reasons: (a) In the austenitic steel analyzed by

Stringfellow *et al.* (1992), the martensitic transformation is strain-induced, i.e., it is controlled by the activation of the nucleation sites resulting from slip preceding the transformation. In the b.c.c. beta phase particles dispersed within the gamma TiAl matrix, on the other hand, the martensitic transformation is controlled by the stress-assisted activation of pre-existing nucleation sites. (b) Martensitic transformed can take place in the entire material (homogenous-phase martensitic transformation) in the austenitic steels while in the case of gamma TiAl the transformation can take place only in discrete beta-phase particles (dispersed-phase martensitic transformation). Dispersed-phase materials systems undergoing stress-assisted martensitic transformation have been analyzed so far using only oversimplified phenomenological constitutive models, e.g. Budiansky *et al.* (1983), Hom and McMeeking (1990). Because such models do not account for the basic thermodynamic and kinetic aspects of the martensitic transformation, their use for understanding dispersed-phase transformation-induced phenomena in real material is very limited. We here propose a new constitutive model which describes transformation plasticity accompanying stress-assisted martensitic transformation in metastable particles embedded into a stable non-transforming matrix. All the numerical evaluation based on the model are done for the material system consisting of metastable Ti-Al-V-Fe based b.c.c. beta phase particles embedded into a gamma TiAl matrix. This alloy system has been recently investigated experimentally by Grujicic and Dang (1996).

Notation used in the present paper is based on the following conventions: Scalars are written in italic (e.g., f, γ, σ), vectors boldface lowercase Roman (e.g., **e, t**), second order tensors as boldface uppercase (e.g., **T, D**), while fourth order tensor using capital boldface italics (e.g., ***I, J***). Tensor (dyadic) products are indicated by '$\otimes$', tensor scalar products of appropriate order by a raised dot. The norm and the transpose of a second order tensor **A** are denoted by $\|\mathbf{A}\|$ and $\mathbf{A}^{\mathrm{T}}$, respectively.

The organization of the paper is as following: in the next section, a fundamental thermodynamics/kinetics based analysis of stress-induced martensitic transformation, and the resulting materials constitutive relations are presented. This is followed by two sections in which the constitutive model is applied to the gamma TiAl/beta (Ti-Al-V-Fe) and the beta/alpha Ti-10V-2Fe-3Al (wt.%) material systems in order to rationalize the experimentally observed enhanced ductility and a sigmoidal stress–strain curves resulting from the martensitic transformation in the beta phase.

FORMULATION

Martensitic transformation in small particles

A decade ago, Olson *et al.* (1987) introduces a constitutive model for polycrystalline materials containing dispersed particles which undergo a martensitic transformation under the influence of an applied stress. Since the model of Olson *et al.* (the OTC model in the following) represents the starting point in the derivation of the materials constitutive model carried out in the present work, it is briefly reviewed here.

In the OTC model, the results of the small particle martensitic transformation experiments carried out by Cech and Turnbull (1956) were used to assess the basic statistics of the heterogeneous nucleation process based on a phenomenologically derived distribution of nucleation site potencies in Fe-30Ni. Under the assumption of a random distribution of the orientation of the (pre-existing) nucleation sites, the effect of an applied stress on the site potency and its distribution was evaluated and, in turn, the observed nonlinear stress dependence of the transformation kinetics was accounted for. The results of the small-particle experiments showed that a fraction, f, of the Fe-30Ni particles which contain a detectable amount of martensitic after cooling to various subambient temperatures is a function of the average particle size and temperature. In the OTC model, the transformed fraction f of the particles containing detectable amount of martensite is equated to the probability p that each of such particles of volume V_p contains at least one nucleation site, as:

$$p = 1 - \exp(-N_v V_p) \tag{1}$$

where N_v is the number density of the nucleation sites randomly distributed throughout the material. By fitting the data of Cech and Turnbull to eqn (1), Olson *et al.* (1987) determined a relationship between the number density of the nucleation sites N_v and the temperature T. Furthermore, using the available transformation thermodynamics data, the number density of nucleation sites was related to the chemical Gibbs free energy change, Δg, which accompanies the f.c.c. → b.c.c. martensitic transformation in Fe-30Ni. Next, using a simple model of barrierless heterogeneous classical martensitic nucleation via elastic interaction of the martensitic nucleus with superdislocation-like linear defects, the potency of a nucleation site operating at a given volume Gibbs free energy change Δg is expressed in terms of a defect size parameter, n, as follows:

$$n = \frac{-2\Gamma/\rho}{\Delta g + g^{el} + w_f}. \tag{2}$$

The size parameter n corresponds to the number of dislocations in the superdislocation-like defect, Γ is the nucleus/matrix specific interfacial energy, ρ is the planar atomic density of the close packed planes, g^{el} is the (coherent) elastic nucleus misfit strain energy, and w_f the frictional work of nucleus/matrix interfacial motion.

The cumulative defect potency distribution of nucleation sites, $N_v(n)$, was determined using the phenomenological approach proposed by Chen *et al.* (1985) as:

$$N_v(n) = N_v^0 \exp(-\alpha n) \tag{3}$$

where α is a constant distribution shape factor, and N_v^0 the total number density of defects of all potencies. The form of eqn (3) is typical of experimentally observed distribution functions for sparsely distributed non-equilibrium structural defects encountered in fracture and fatigue. Substitution of eqn (2) into eqn (3) yields:

$$N_v(n) = N_v^0 \exp\left(\frac{-2\alpha\Gamma/\rho}{\Delta g + g^{el} + w_f}\right) \tag{4}$$

which represents the thermodynamic (structural) nucleation site potency distribution function, as introduced by the OTC model.

Martensitic transformation-controlled deformation

Orientation dependence of the mechanical driving force. When the martensitic transformation occurs under an applied stress, as originally treated by Patel and Cohen (1953), the total Gibbs free energy change accompanying the transformation or the driving force for transformation, Δg, is the sum of the chemical contribution Δg^{ch} and a mechanical contribution Δg^{σ}. The Δg^{σ} contribution is a nucleus orientation dependent quantity and can be expressed in terms of the stress normal to the transformation habit plane, σ_n, and the shear stress in this plane resolved in the direction of transformation strain, τ, and is expressed by:

$$\Delta g^{\sigma} = \sigma_n \varepsilon_0 + \tau \gamma_0 \tag{5}$$

where ε_0 and γ_0 are the normal and shear transformation strains, respectively, which are both characteristics of the given alloy system. If the applied stress tensor, expressed in a global coordinate system, is denoted by **T**, the resolved normal and shear stresses associated with a given transformation system (the habit plane and the direction of transformation shear) can be obtained as:

$$\sigma_n = \mathbf{N}_{global} \cdot \mathbf{T} \tag{6a}$$

$$\tau = \mathbf{R}_{global} \cdot \mathbf{T} \tag{6b}$$

where $\mathbf{R}_{global}$ and $\mathbf{N}_{global}$ (both expressed in the global coordinate system) are called the transformation tensors and are defined in terms of the corresponding Euler angles (θ, ϕ, ψ) as:

$$\mathbf{R}_{global}(\theta, \phi, \psi) = \mathbf{P}(\theta, \phi, \psi)\mathbf{R}_{local}\mathbf{P}^{\mathrm{T}}(\theta, \phi, \psi) \tag{7a}$$

$$\mathbf{N}_{global}(\theta, \phi, \psi) = \mathbf{P}(\theta, \phi, \psi)\mathbf{N}_{local}\mathbf{P}^{\mathrm{T}}(\theta, \phi, \psi) \tag{7b}$$

where $\mathbf{R}_{local}$, the symmetric part of the Schmid tensor, and $\mathbf{N}_{local}$ are two tensors defined in terms of the habit plane normal $\mathbf{n}$ and the transformation shear direction $\mathbf{b}$ of a given transformation system, both expressed within a local coordinate system as:

$$\mathbf{R}_{local} = \tfrac{1}{2}[(\mathbf{n} \otimes \mathbf{b}) + (\mathbf{b} \otimes \mathbf{n})] \tag{8a}$$

and

$$\mathbf{N}_{local} = \mathbf{n} \otimes \mathbf{n}. \tag{8b}$$

The local to global transformation matrix $\mathbf{P}$ as used in eqns (7a) and (7b) is defined in terms of the Euler angles (θ, ϕ, ψ), as:

$$\mathbf{P}(\theta, \phi, \psi) = \begin{bmatrix} \cos\psi\cos\phi\cos\theta - \sin\phi\sin\theta & -\cos\psi\sin\phi - \sin\psi\cos\theta\cos\phi & \sin\theta\cos\phi \\ \cos\psi\cos\theta\sin\phi + \sin\psi\cos\phi & -\sin\psi\cos\theta\sin\phi + \cos\psi\cos\phi & \sin\theta\sin\phi \\ -\cos\psi\sin\theta & \sin\psi\sin\theta & \cos\theta \end{bmatrix}. \tag{9}$$

The use of eqns (5)–(9) for any applied stress state yields the mechanical driving force in a (stress-state dependent) range between Δg^{σ}_{min} and Δg^{σ}_{max}. The distribution of the mechanical driving force in such a range (i.e., the mechanical driving force probability density vs the mechanical driving force function) can be determined analytically only in the cases of a relatively simple applied stress states. The results of an analytical procedure for the cases of uniaxial tension and compression obtained by Sankaran (1996) are given in Fig. 1. When the mechanical driving force distribution function cannot be determined

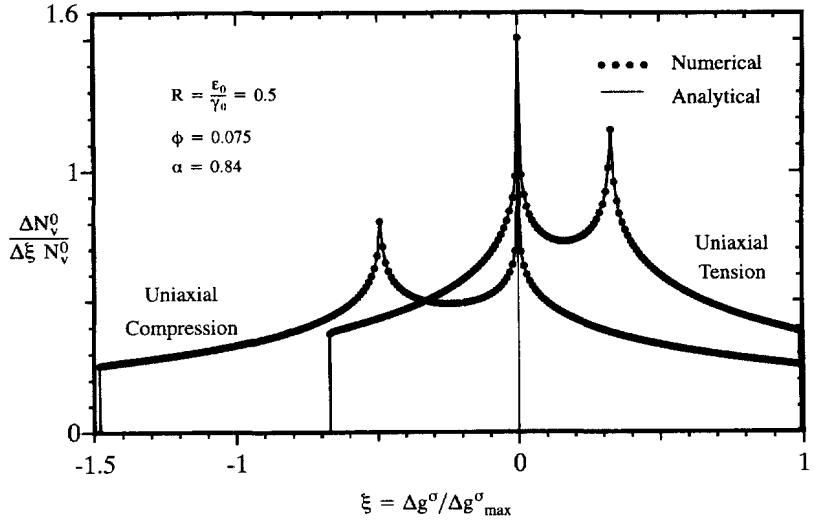

Fig. 1. The probability density function of the normalized mechanical driving force for uniaxial tension and uniaxial compression.

analytically, a numerical procedure can be utilized. Within such a procedure, Δg^{σ} is evaluated using eqns (5)–(9) over a very fine mesh in the (θ, ϕ, ψ) space, and a histogram constructed giving the number of points lying in small intervals of Δg^{σ}. The probability density function $F(\Delta g^{\sigma}) = 1/N_v^0[\mathrm{d}N_v(\Delta g^{\sigma})/\mathrm{d}\Delta g^{\sigma}]$ is next numerically normalized, so that:

$$\int_{\Delta g^{\sigma}_{min}}^{\Delta g^{\sigma}_{max}} \frac{\mathrm{d}N_v^0(\Delta g^{\sigma})}{N_v^0\,\mathrm{d}\Delta g^{\sigma}}\mathrm{d}\Delta g^{\sigma} = \int_{\Delta g^{\sigma}_{min}}^{\Delta g^{\sigma}_{max}} F(\Delta g^{\sigma})\,\mathrm{d}\Delta g^{\sigma} = 1. \tag{10}$$

A normalized mechanical driving force $\xi = \Delta g^{\sigma}/\Delta g^{\sigma}_{max}$ is used in Fig. 1 and consequently the probability density function expressed as $F(\xi) = \mathrm{d}N_v^0(\xi)/\mathrm{d}\xi N_v^0$.

The numerical procedure for the computation of the normalized mechanical driving force probability density described above, is applied to the cases of uniaxial tension and compression, for a value of the transformation strain ratio $R = \varepsilon_0/\gamma_0 = 0.04/0.08 = 0.5$ (the values $\varepsilon_0 = 0.04$ and $\gamma_0 = 0.08$ are typical to the Ti-based system being considered here, Grujicic and Narayan (1992)) and $\Delta\xi = 10^{-2}$. The results of this calculation are shown in Fig. 1 and are practically identical with the analytical results obtained by Sankaran (1996). While the analytical procedure is preferred because of its higher accuracy, it becomes intractable for complicated stress states and the proposed numerical procedure has to be applied.

The results given in Fig. 1 show that due to the positive character of the dilatational term ε_0, the distribution has two peaks whose location is determined by the magnitude of the transformation strain ratio R. The displacement of the distribution centers relative to $\xi = 0$, indicates that, due to the fact that $\varepsilon_0 > 0$, the nucleation sites subject to a positive mechanical driving force ξ are more plentiful than those subject to negative ξ in the case of tension, and vice versa in the case of compression. The opposite is true for the negative ε_0 case.

Cumulative operational nucleation site potency distribution. For any given distribution of nucleation-site orientations such as the random distribution, the cumulative operational nucleation-site potency distribution expressed in terms of the applied stress required for site operation will be broadened relative to the structural potency distribution of eqn (3) due to the distribution of the mechanical driving force (e.g., Fig. 1). In the case of a random distribution, this broadening can be predicted from the mechanical driving force distribution associated with a given stress state, e.g., Fig. 1, as follows:

$$N_v(\Delta g^{ch}, \mathbf{T}) = N_v^0 \int_{\Delta g^{\sigma}_{min}}^{0} \frac{\mathrm{d}N_v^0(\Delta g^{\sigma})/N_v^0}{\mathrm{d}\Delta g^{\sigma}} \exp\left(\frac{2\alpha\Gamma/\rho}{\Delta g^{ch} + g^{el} + w_f}\right)\mathrm{d}\Delta g^{\sigma}$$
$$+ N_v^0 \int_{0}^{\Delta g^{\sigma}_{max}} \frac{\mathrm{d}N_v^0(\Delta g^{\sigma})/N_v^0}{\mathrm{d}\Delta g^{\sigma}} \exp\left(\frac{2\alpha\Gamma/\rho}{\Delta g^{ch} + \Delta g^{\sigma}(\mathbf{T}) + g^{el} + w_f}\right)\mathrm{d}\Delta g^{\sigma} \tag{11}$$

where $N_v(\Delta g^{ch}, \mathbf{T})$ is the cumulative operational nucleation site distribution function associated with the applied stress $\mathbf{T}$, under the assumption that the external stress is applied under isothermal conditions and that the martensitic transformation is an irreversible process. The integrands in eqn (11) represent the fractions of the operational nucleation sites relative to total number of nucleation sites, subject to the mechanical driving forces between Δg^{σ} and $\Delta g^{\sigma} + \mathrm{d}\Delta g^{\sigma}$ associated with the externally applied stress state $\mathbf{T}$. The function given by eqn (11) can be readily evaluated using numerical integration. The results of such a numerical integration procedure for the cases of uniaxial tension and uniaxial compression, at $\phi = 0.09$, $\varepsilon_0/\gamma_0 = 0.5$ and $\alpha = 0.84$ (typical for the Ti-base system, Grujicic and Narayan (1992)) are shown in Fig. 2. The normalized chemical driving force, ϕ, is defined as:

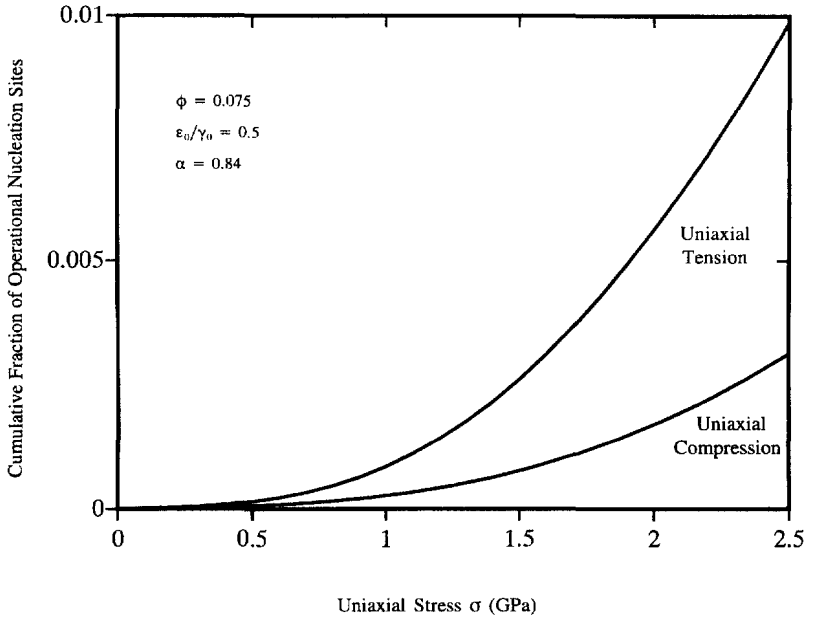

Fig. 2. Cumulative fraction of operational nucleation sites as a function of the applied stress.

$$\phi = -\frac{\Delta g^{ch} + g^{el} + w_f}{2\Gamma/\rho}. \tag{12}$$

The results demonstrate, that at the same magnitude of the applied uniaxial stress, a larger fraction of nucleation sites becomes operational in the case of uniaxial tension than in the case of uniaxial compression. This result is consistent with the fact that since $\varepsilon_0 > 0$, the positive hydrostatic stress in the case of uniaxial tension promotes transformation while negative hydrostatic stress in the case of uniaxial compression opposes the transformation.

Transformation-controlled yield surface. The yield criterion specifies the condition in a multi-axial stress state at which plastic flow starts. In the case of a transforming phase, this condition is assumed to be achieved, when a critical number of nucleation sites become operational. For any given multiaxial stress state, the number of operational nucleation sites, $N_v(\Delta g^{ch}, \mathbf{T})$, can be calculated using eqn (11). Conversely, if a fixed number of operational nucleation sites, N_v^c, is assumed to correspond to the onset of plastic flow, eqn (11) can be used to calculate the magnitude of stress components for any multiaxial stress state required to make this many nucleation sites operational. Representing such yield conditions in the stress space for a large number of stress states can be used to determine the transformation yield surface.

The procedure for determination of the yield surface discussed above, is next applied to find the yield locus for the biaxial stress states. The critical number of operational nucleation sites was set equal to 1×10^6–5×10^6 cm^{-3}, which is the range often cited to correspond to the onset of martensitic transformation at the M_s (martensitic start) temperature during cooling, Olson *et al.* (1987). The results of this calculation are shown in Fig. 3.

To better understand the character of biaxial transformation yield locus, the results shown in Fig. 3 are replotted using the stress invariants (the effective deviatoric stress, $\bar{\sigma}$, and the hydrostatic stress, σ_h) as following: For each point on the transformation yield locus characterized by σ_1 and σ_2, the effective deviatoric stress, $\bar{\sigma} = \sqrt{\sigma_1^2 + \sigma_2^2 - \sigma_1\sigma_2}$ and the corresponding hydrostatic stress, $\sigma_h = (\sigma_1 + \sigma_2)/3$ are computed, and in turn a $\bar{\sigma}$ vs σ_h plot generated. The results of this procedure are shown in Fig. 4. The results indicate that, except at large negative hydrostatic stresses, a fairly linear relationship exists between the two stress invariants, $\bar{\sigma}$ and σ_h, and hence the biaxial transformation yield condition can be simplified as:

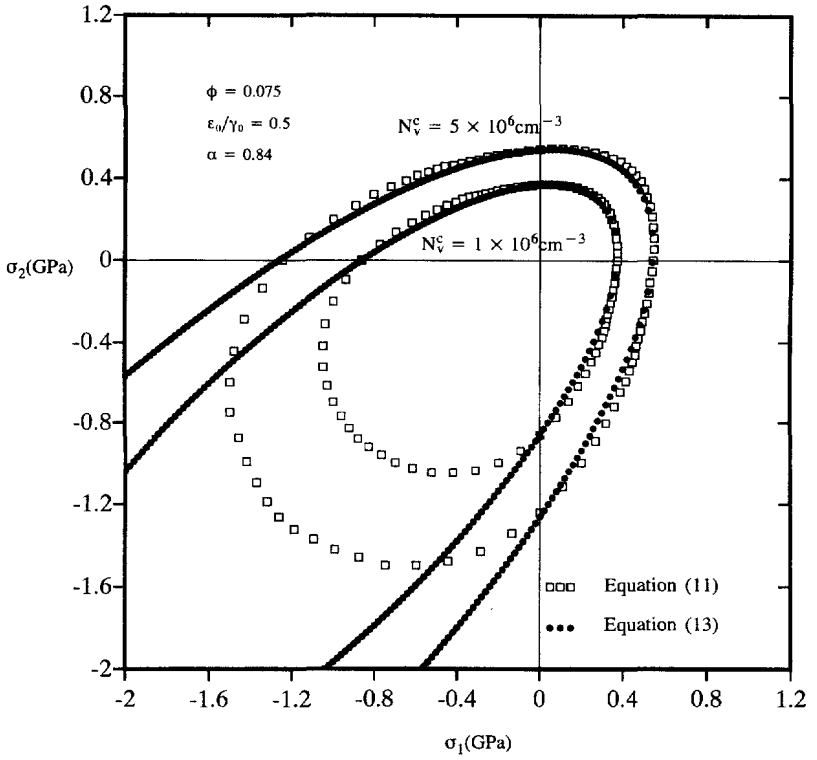

Fig. 3. Transformation yield loci associated with two different fixed numbers of activated nucleation sites.

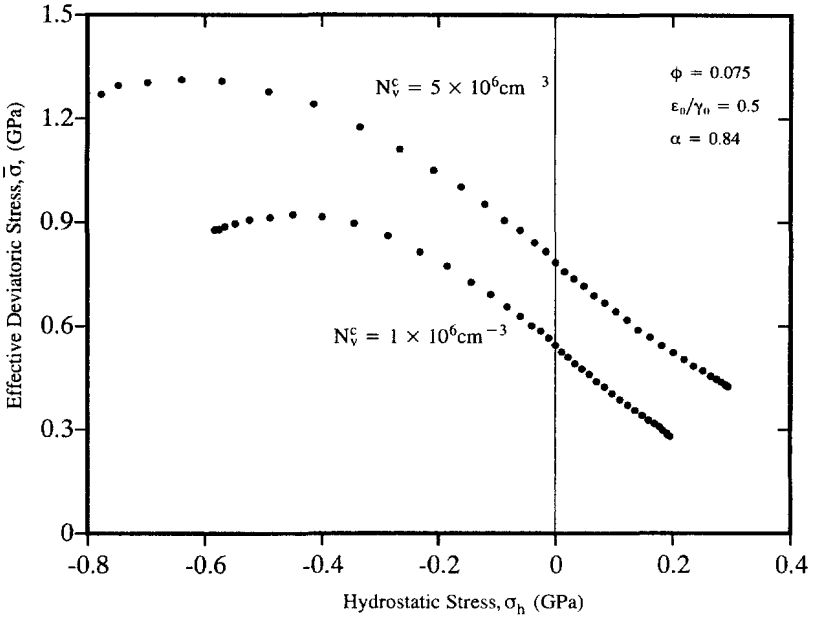

Fig. 4. Relation between the stress invariants, $\bar{\sigma}$ and σ_h, along the yield loci shown in Fig. 3.

$$\bar{\sigma} = \sigma_s - k^* \sigma_h \tag{13}$$

where σ_s corresponds to the effective deviatoric yield stress in pure shear ($\sigma_h = 0$), and k^* is the hydrostatic stress sensitivity coefficient. Both σ_s and k^* are expected, in general, to be a function of N_v^c. However, the results shown in Fig. 4, suggest that k^* is approximately constant for $N_v^c = 1 \times 10^6 - 5 \times 10^6$ cm^{-3} and equal to 1.2 ± 0.05. Furthermore, by applying eqn (11) to a number of triaxial stress states associated with a positive hydrostatic stress, it

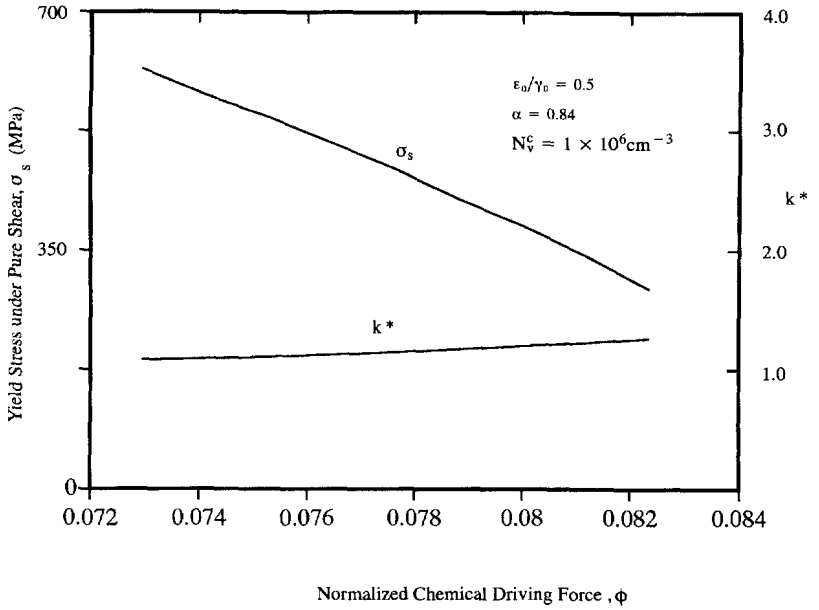

Fig. 5. Effect of the normalized chemical driving force on the yield stress in pure shear, and on the hydrostatic stress sensitivity coefficient, k^*.

was found that the yield condition given by eqn (13), also holds for such triaxial stress states.

The yield condition given by eqn (13) states that, in the σ_1–σ_2–σ_3 principal coordinate system, the yield surface represents a cone whose axis is aligned along the hydrostatic stress $\sigma_1 = \sigma_2 = \sigma_3$ line, and whose apex is at $\sigma_h = \sigma_s/k^*$. As the transformation proceeds (σ_s increases, k^* remains approximately constant), the cone expands in such a way that its axis remains along the $\sigma_1 = \sigma_2 = \sigma_3$ line. The two-dimensional yield loci (ellipses) corresponding to the yield cone and $N_v^c = 1 \times 10^6$ and $N_v^c = 5 \times 10^6$ cm^{-3} are also shown in Fig. 4. As expected, reasonable agreement between the actual and simplified yield loci is obtained only in the region associated with positive values of the hydrostatic stress.

The results shown in Fig. 4 and eqn (13) show that, in contrast to the plastic deformation by slip or twinning, the yield criterion for the martensitic transformation controlled plasticity is affected by the hydrostatic stress. This phenomenon is the result of a coupling between the hydrostatic stress and the volume change ε_0 accompanying the martensitic transformation.

The results shown in Fig. 4 and the reported values for σ_s and k^* are associated with a fixed value of the chemical driving force ($\phi = 0.075$). Since ϕ is a measure of the thermodynamic stability of the transforming phase, σ_s (and perhaps k^*) are expected to depend on ϕ. This is confirmed by the results shown in Fig. 5, where σ_s is found to be a strong function of ϕ. k^*, on the other hand, is only weakly dependent on ϕ. The observed variation of σ_s with ϕ is expected because, as the transforming phase becomes less stable (ϕ increases), the transformation requires a lower level of the applied stress, σ_s, to proceed.

Evolution of martensite under applied stress. If the number of transforming phase particles is large, the fraction of particles transformed to martensite can be described by the probability p given in eqn (1). Consequently, by combining eqns (1) and (10), under the condition of isothermal loading to a stress level, $\mathbf{T}$, the transformed fraction, f, can be expressed as:

$$f(\mathbf{T}) = 1 - \exp[N_v(\mathbf{T})V_p]. \tag{14}$$

Equation (14) is next used to determine the transformed fraction of particles corresponding to the onset of transformation controlled plastic deformation, when

$N_v^c = 1 \times 10^6 - 5 \times 10^6$ cm^{-3}. This procedure yields f in the range between 0.005 and 0.02. Equation (14) pertains to the case when the stress of any level is applied instantaneously and hence neglects the fact that the number of nucleation sites which are most favorably oriented relative to the applied stress field and which thus dominate the transformation kinetics at lower volume fractions of martensite, decreases as the transformation proceeds. To handle this problem, the evolution of transformed fraction of the particles with the stress has to be analyzed in an incremental fashion. Towards that end, the probability that a particle will transform when the stress state is incremental between $\mathbf{T}_n$ and $\mathbf{T}_{n+1}$ is introduced as:

$$\Delta p_n = 1 - \exp[-\{N_v(\mathbf{T}_{n+1}) - N_v(\mathbf{T}_n)\} V_p]. \tag{15}$$

The number of operational nucleation sites at two levels of applied stress, $N_v(\mathbf{T}_{n+1})$ and $N_v(\mathbf{T}_n)$, are determined through the use of eqn (11). The corresponding increment in the transformed fraction of particles is:

$$\Delta f_n = (1 - f_n)\Delta p_n \tag{16}$$

where the $(1-f_n)$ term takes into account the fact that due to the previously applied stress $\mathbf{T}_n$, only a $(1-f_n)$ fraction of the original transforming phase particles is available for transformation when the stress is incremented to $\mathbf{T}_{n+1}$. The total transformed fraction after $n+1$ increments in stress is then obtained by simply adding the incremental transformed fraction, Δf_n, to the total transformed fraction after n increments in stress, i.e.:

$$f_{n+1} = f_n + \Delta f_n. \tag{17}$$

The evolution of martensite resulting from the monotonically applied stress, as governed by eqns (15)–(17), the transformed fraction as a function of the stress magnitude is computed for the cases of uniaxial tension and uniaxial compression and the results depicted in Fig. (6). Also shown in Fig. 6, is a martensite evolution curve corresponding to the applied uniaxial tensile stress case associated with a fixed and maximum level of the mechanical driving force as given by $\Delta_g^\sigma = \Delta g_{max}^{\sigma,ut} = -\sigma/2[\sqrt{\gamma_0^2 + \varepsilon_0^2} + \varepsilon_0]$. This curve corresponds to the case when the operational transformation system in all the particles are of

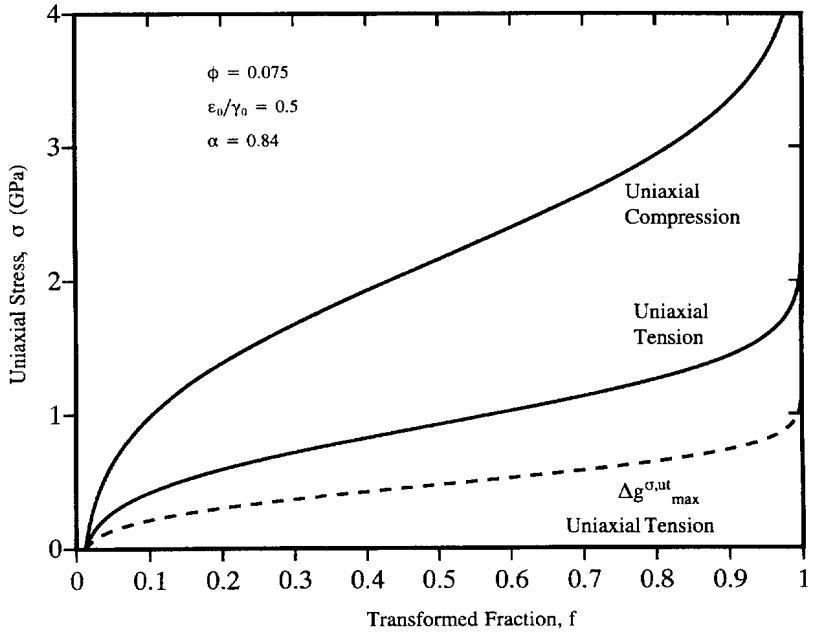

Fig. 6. Relationship between the transformed fraction of the transforming phase particles, f, as a function of the magnitude of the applied stress, σ.

the same orientation, the orientation which is associated with the maximum effect of the mechanical driving force for transformation. The σ vs f curve is in this case defined by the following relationship, obtained by combining eqn (14) and (4):

$$f(\sigma) = 1 - \exp\left[- V_p N_v^0 \exp\left(\frac{2\alpha\Gamma/\rho}{\Delta g^{ch} + \Delta g^{\sigma}_{max}(\sigma) + g^{el} + w_f} \right) \right]. \tag{18}$$

Using the aforementioned definition of $\Delta g^{\sigma,ut}_{max}$, eqn (17) can be rewritten as:

$$f = 1 - \exp\left[- V_p N_v^0 \exp\left(\frac{2\alpha\Gamma/\rho}{\Delta g^{ch} - \frac{\sigma_{\Delta g^{\sigma}_{max}}}{2}(\sqrt{\gamma_0^2 + \varepsilon_0^2} + \gamma_0) + g^{el} + w_f} \right) \right]. \tag{19}$$

All three curves in Fig. 6 were obtained using the same set of parameters characteristic of the Ti-base system under consideration ($N_v^0 = 2 \times 10^{17}$, $V_p = 10^3$, $\alpha = 0.84$, $\Gamma = 0.15$ J/m^2, $\rho = 3.01 \times 10^5$ mol/m^2, $g^{el} + w_f = 180$ J/mol, $\Delta g^{ch} = -800$ J/mol, Sankaran (1996)).

Equation (19) is next inverted to give a relationship between the uniaxial tensile stress and the transformed fraction under the condition $\Delta g^{\sigma} = \Delta g^{\sigma,ut}_{max}$ as:

$$\sigma_{\Delta g^{\sigma,ut}_{max}}(f) = \frac{2}{\sqrt{\gamma_0^2 + \varepsilon_0^2} + \gamma_0} \left[\frac{2\alpha\Gamma/\rho}{\ln\left[\frac{1}{-V_p N_v^0} \ln(1-f) \right]} - \Delta g^{ch} - g^{el} - w_f \right]. \tag{20}$$

Because of the similarity in the shape of the $\Delta g^{\sigma} = \Delta g^{\sigma,ut}_{max}$ stress vs transformed fraction curve and the ones for uniaxial tension and uniaxial compression corresponding to the random orientation of nucleation sites, the latter are related to the former via the following simple expressions:

$$\sigma^{ut} = \beta^{ut} \sigma_{\Delta g^{\sigma}_{max}} \tag{21a}$$

and

$$\sigma^{uc} = \beta^{uc} \sigma_{\Delta g^{\sigma}_{max}} \tag{21b}$$

where σ^{ut} and σ^{uc} are respectively the uniaxial tensile stress and the uniaxial compression stress corresponding to the case of a random distribution of nucleation sites. β^{ut} and β^{uc} are the corresponding scaling factors that account for the random distribution of nucleation sites and both are, in general, a function of the transformed fraction of the particles. However, for the results shown in Fig. 6, it is found that β^{ut} and β^{uc} are practically constant and, respectively, equal to 1.95 and -4.55.

In view of the fact that a constant level of f (i.e., N_v^c = constant) is associated with a fixed value of the deviatoric yield stress in pure shear, in eqn (13), σ_s is renamed the yield resistance, R, and is next expressed in terms of the transformed fraction of particles using eqns (20) and (21a) or (21b) as:

$$\begin{aligned} R(f) &= \bar{\sigma} + k^* \sigma_h \\ &= \frac{2\beta}{\sqrt{\gamma_0^2 + \varepsilon_0^2} + \gamma_0} \left[\frac{2\alpha\Gamma/\rho}{\ln\left[\frac{1}{-V_p N_v^0} \ln(1-f) \right]} - \Delta g^{ch} - g^{el} - w_f \right] \end{aligned} \tag{22}$$

where

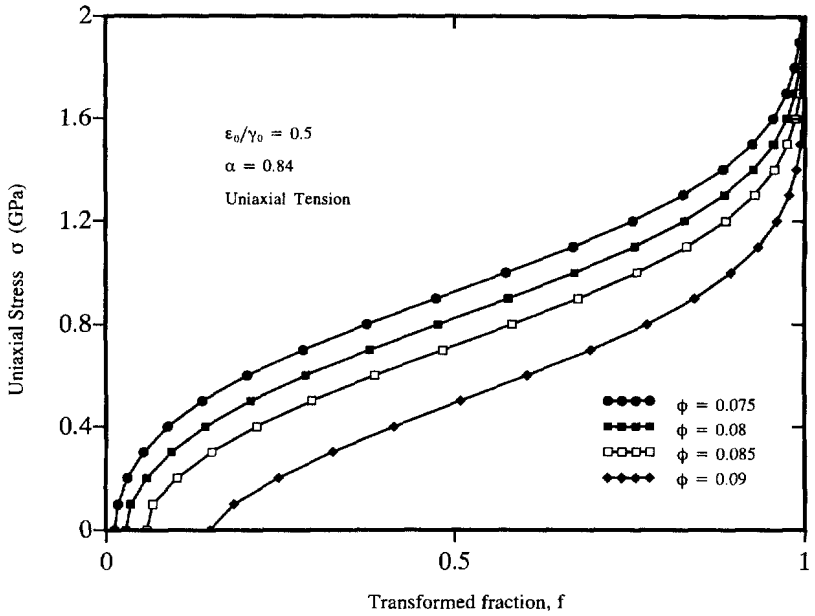

Fig. 7. Effect of the normalized chemical driving force, ϕ, on the progress of martensitic transformation during uniaxial tensile loading.

$$\beta = \beta^{ut}\left(1+\frac{k^*}{3}\right) = \beta^{uc}\left(1-\frac{k^*}{3}\right) = 2.73. \tag{23}$$

The terms $+k^*/3$ and $-k^*/3$ in eqn (23) come from the fact that $\sigma_h = \bar{\sigma}/3$ for uniaxial tension and $\sigma_h = -\bar{\sigma}/3$ for uniaxial compression.

The effect of the thermodynamic stability of the transforming phase on the progress of martensitic transformation under the applied uniaxial tensile stress for four different levels of the chemical driving force in the range between $\phi = 0.075$ and $\phi = 0.090$ is displayed in Fig. 7. As expected, an increase in the chemical driving force for transformation gives rise to a larger transformed fraction of the transforming phase particles at each level of the applied stress, including the initial zero-stress level, at which the transformation is the result of the chemical driving force alone.

Evolution of transformation plastic strain. The plastic strain due to martensitic transformation in the absence of any applied stress and in the absence of any morphological and crystallographic texture is expected to be isotropic and hence is purely dilatational in nature. Assuming that no load is applied till time $t = 0$, the corresponding strain due to the transformation is given by:

$$\bar{\varepsilon}^p_{t=0} = f_0 \frac{\varepsilon_0}{3}\mathbf{I} \tag{24}$$

where f_0 is the transformed fraction at time $t = 0$, evaluated using eqns (11) and (14).

The evolution of plastic strain during loading ($t > 0$) can be evaluated by taking into account the history of the loading. For instance, under the assumption of a random distribution of nucleation sites, the increase in the macroscopic plastic strain resulting from the transformed fraction due to the increment in stress between $\mathbf{T}_n$ and $\mathbf{T}_{n+1}$ can be obtained by summing the contribution of all the particles transformed as a result of this stress increment as:

$$\Delta\varepsilon_n^p = \frac{\Delta f_n \int_0^{2\pi}\int_0^{2\pi}\int_0^{\pi} \varepsilon_{p,n+1}^p(\theta,\phi,\psi)P_{p,n+1}(\theta,\phi,\psi)\sin\theta\,\mathrm{d}\theta\,\mathrm{d}\phi\,\mathrm{d}\psi}{\int_0^{2\pi}\int_0^{2\pi}\int_0^{\pi} P_{p,n+1}(\theta,\phi,\psi)\sin\theta\,\mathrm{d}\theta\,\mathrm{d}\phi\,\mathrm{d}\psi} \tag{25}$$

where $\varepsilon_{p,n+1}^p$ is the strain (expressed in the global coordinate system) associated with a transformed particle p, $P_{p,n+1}(\theta, \phi, \psi)$ is the loading history dependent probability that a particle p has transformed as a result of a stress increase between $\mathbf{T}_n$ and $\mathbf{T}_{n+1}$, by the operation of a nucleation site associated with the Euler angles θ, ϕ and ψ. Due to the orientation dependence of the mechanical driving force, as defined by eqns (5)–(9), the probability $P_{p,n+1}$ can be related to the probability that a nucleation site associated with the Euler angles θ, ϕ and ψ subject to the stress level $\mathbf{T}_{n+1}$ will become operational as follows:

$$P_{p,n+1}(\theta,\phi,\psi) = \bar{P}\exp\left(\frac{2\alpha\Gamma/\rho}{\Delta g^{\sigma}(\mathbf{T}_{n+1},\theta,\phi,\psi)+\Delta g^{ch}+g^{el}+w_f}\right)\Delta g^{\sigma} < 0 \tag{26a}$$

and

$$P_{p,n+1}(\theta,\phi,\psi) = 0 \quad \Delta g^{\sigma} \geqslant 0 \tag{26b}$$

where the $\bar{P}_n$ term on the right hand side of eqn (26a) accounts for the fact that due to prior transformation, only a fraction of the initial nucleation sites associated with the Euler angles θ, ϕ and ψ is available for transformation when the stress is incremented between $\mathbf{T}_n$ and $\mathbf{T}_{n+1}$. This loading-history dependent term can be derived using a simple analysis based on eqn (4) and is given by the expression:

$$\bar{P}_n(\theta,\phi,\psi) = \prod_{i=0}^{n}\left[1-\exp\left(\frac{2\alpha\Gamma/\rho}{\Delta g^{\sigma}(\mathbf{T}_i,\theta,\phi,\psi)+\Delta g^{ch}+g^{el}+w_f}\right)\right] \tag{27}$$

where the initial stress $\mathbf{T}_0 = 0$ and the stress is incremented as $\mathbf{T}_{i+1} = \mathbf{T}_i + \Delta\mathbf{T}_i$. The second term on the right hand side of eqn (26a) represents the probability that a nucleation site that is associated with the Euler angles θ, ϕ and ψ will transform when subject to a stress level $\mathbf{T}_{n+1}$.

To evaluate eqn (25), the Euler space was divided into $N = 8000$ regions using $N_\theta = 20$ uniform intervals of θ, $N_\phi = 20$ uniform intervals of ϕ, and $N_\psi = 20$ uniform intervals of ψ, such that $N_\theta \times N_\phi \times N_\psi = N$. Consequently, eqn (25) is expressed as:

$$\Delta\bar{\varepsilon}_n^p = \Delta f_n \frac{\sum_{i=1}^{N} \varepsilon_{i,n+1}^p / P_{p,n+1}^i \sin\theta_i}{\sum_{i=1}^{N} P_{p,n+1}^i \sin\theta_i} \tag{28}$$

where the probability for transformation of the particles in the i-th region of the Euler space, $P_{p,n+1}^i$, is defined as the probability that a nucleation site associated with the Euler angles corresponding to this region is activated. This probability is given by eqns (26a) and (26b), depending on the sign of the corresponding mechanical driving force.

The contribution of complete transformation of a particle in the i-th region of the Euler space to the macroscopic plastic strain, $\varepsilon_{i,n+1}$, as appearing in eqn (28) is given by:

$$\varepsilon^p_{i,n+1}(\theta, \phi, \psi) = \gamma_0 \mathbf{R}^i_{global} + \varepsilon_0 \mathbf{N}^i_{global} \tag{29}$$

where $\mathbf{R}_{global}$ and $\mathbf{N}_{global}$ are defined in terms of the Euler angles of the particular transformation system, and are given by eqns (7)–(9). To complete the calculations given in eqn (28), the increment in the transformed fraction, Δf_n, has to be calculated using eqn (16).

To compute the total plastic strain associated with the stress level $\mathbf{T}_{n+1}$, namely ε^p_{n+1}, the plastic strain increment computed using eqn (25), $\Delta\varepsilon^p_n$, should be added to the total plastic strain corresponding to the stress level $\mathbf{T}_n$, as following:

$$\varepsilon^p_{n+1} = \varepsilon^p_n + \Delta\varepsilon^p_n. \tag{30}$$

The procedure just described allows determination of the evolution of the transformation plastic strain tensor during loading. Furthermore, the plastic strain tensor given in eqn (30) can be decomposed into its deviatoric and hydrostatic parts as:

$$\varepsilon^p_{n+1} = \sqrt{\tfrac{3}{2}}\bar{\varepsilon}^p_{n+1}\mathbf{N} + \varepsilon_{h,n+1}\mathbf{I} \tag{31}$$

and this decomposition allows the evolution of these two components of the plastic strain, one describing the shape change, and the other describing the volume change, to be monitored. In eqn (31), $\bar{\varepsilon}^p_{n+1} = \sqrt{2/3(\varepsilon^2_{11} + \varepsilon^2_{22} + \varepsilon^2_{33})}$ is the equivalent plastic strain, $\varepsilon_{h,n+1} = (\varepsilon_{11} + \varepsilon_{22} + \varepsilon_{33})/3$ is the dilatational strain, and ε_{11}, ε_{22} and ε_{33} are the principal components of the plastic strain, ε^p_{n+1}.

The aforementioned procedure for determination of the evolution of the plastic strain is next applied to the specific cases of monotonic loading in uniaxial tension and uniaxial compression. The evolution of the principal plastic strains with uniaxial stress and the evolution of the deviatoric and dilatational components of the plastic strain with uniaxial stress are shown in Figs 8 and 9, respectively.

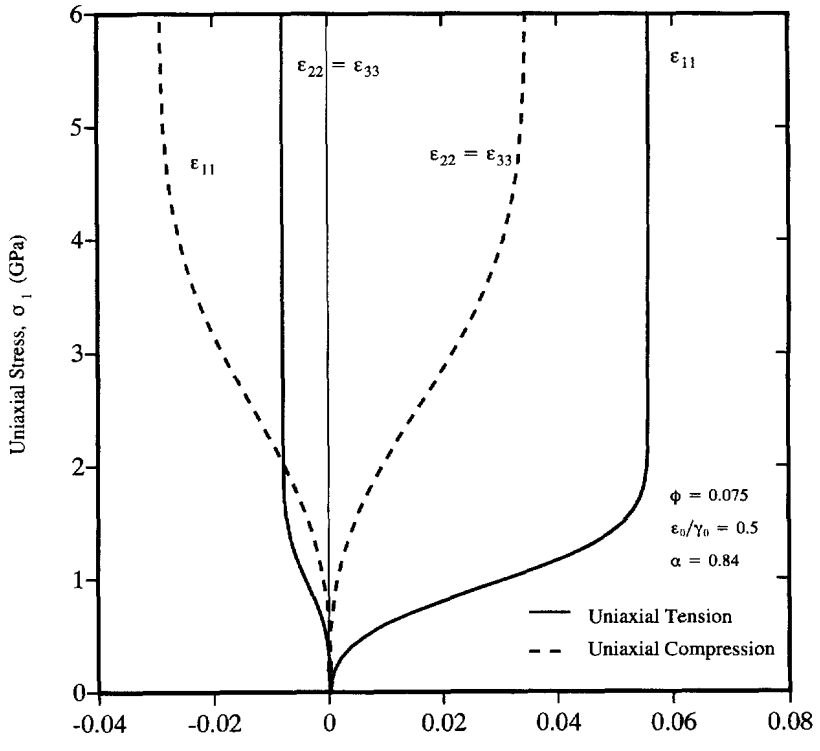

Fig. 8. Evolution of the principal components of the transformation plastic strain for uniaxial tension and uniaxial compression.

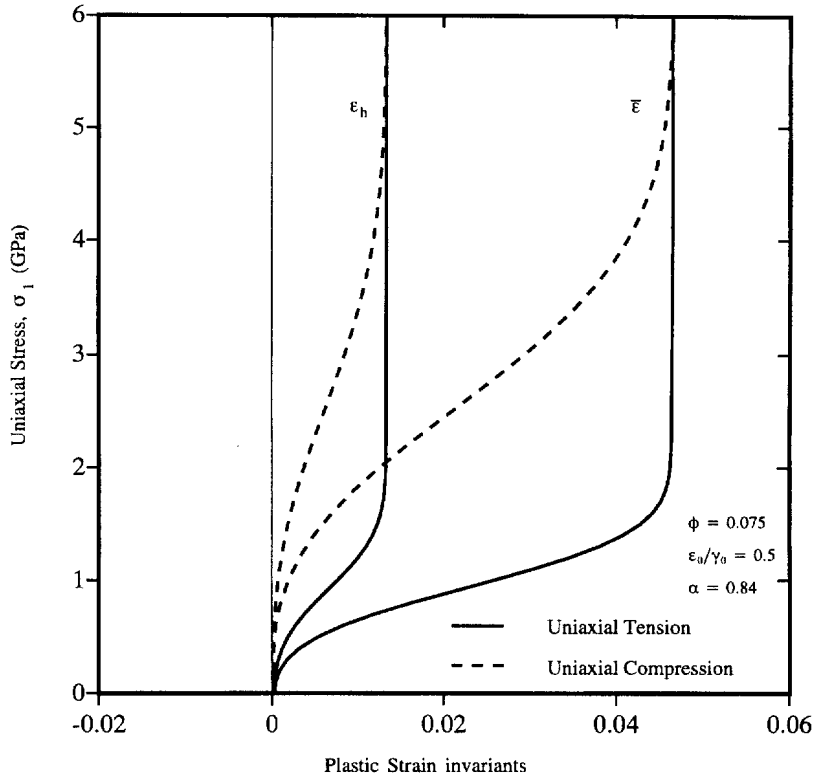

Fig. 9. Evolution of the equivalent and hydrostatic transformation plastic strains for uniaxial tension and uniaxial compression.

The results shown in Figs 8 and 9 indicate that, as expected, the plastic strain increases with increasing magnitude of the applied stress. However, since the particles containing favorably oriented nucleation sites are activated early during the transformation, further progress in transformation, and hence further increments in plastic strain depend on the transformation of particles containing less favorable nucleation sites. As a result, progressively smaller increments in plastic strains for the same increments in stress are observed in the latter stages of transformation. Eventually, the stress becomes extremely high so that other deformation modes such as slip or twinning become dominant.

The results for uniaxial tension and uniaxial compression shown in Figs 6 and 9 are next used to establish a relationship between the equivalent plastic strain, and the transformed fraction of particles. The resulting relationship is shown in Fig. 10 and can be represented as:

$$\bar{\varepsilon} = \varepsilon_1 f - \varepsilon_2. \tag{32}$$

Since ε_2 was found to be very small (1×10^{-4}), it is ignored in the subsequent analysis and, hence, ε_1 is considered as the maximum achievable equivalent plastic strain at the completion of transformation ($f = 1$). The average magnitude of ε_1 for uniaxial tension and uniaxial compression is found to be 0.046. Equation (32) is next used to relate the transformed fraction, corresponding to the onset of transformation controlled plastic deformation ($0.005 < f < 0.02$), to the equivalent plastic strain at the onset of transformation. This resulted in a range of ε values between 2.5×10^{-4} and 1×10^{-3}.

A comparison of the results shown in Figs 8 and 9 suggests that not only the equivalent strain but also the dilatational plastic strain is proportional to the transformed fraction of particles. The maximum dilatational plastic strain corresponding to the completion of martensitic transformation is $\varepsilon_0/3$, where ε_0 is the normal transformation strain. The relationship between the dilatational plastic strain and the transformed fraction of particles can thus be represented as:

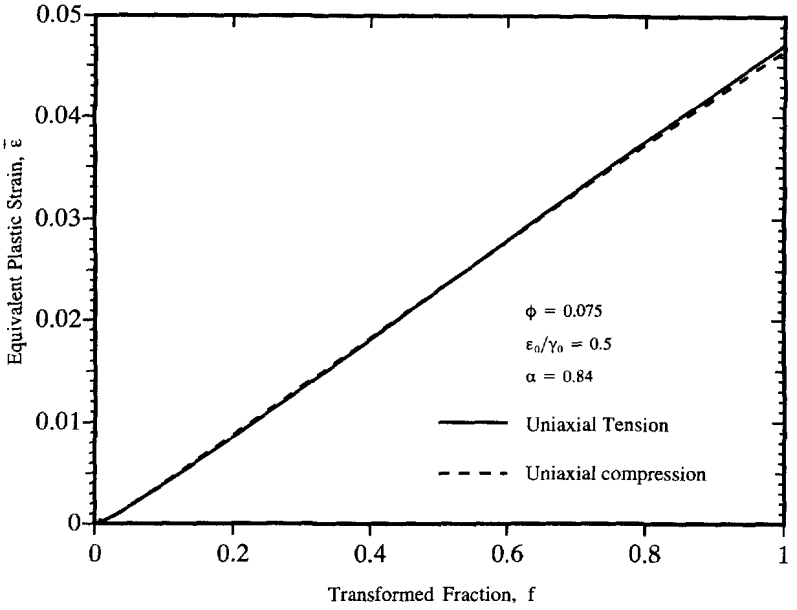

Fig. 10. Relationship between the equivalent transformation plastic strain, $\bar{\varepsilon}$, and the transformed fraction, f.

$$\varepsilon_h = \frac{\varepsilon_0}{3} f. \tag{33}$$

It should be noted that the evolution of the strain carried out in this section is based on the assumption that the strain in a fully transformed particle is equal to that of the associated nucleus. This assumption is typically valid in small particles embedded into a compliant matrix. In larger particles, however, martensitic transformation involves autocatalytic formation of a number of martensitic variants, which tends to decrease the net deviatoric strain. On the other hand, the growth of a single variant is accompanied by accommodation slip in the surrounding parent phase and the bias of this slip tends to increase the deviatoric strain.

Derivation of the materials constitutive relations

Model assumptions. The materials constitutive relations developed in this section are based on the following simplifying assumptions:

(1) The material consists initially of two phases: a transforming phase present in the form of discrete particles embedded into a stable (non-transforming) matrix phase.

(2) Each material point is assumed to contain the appropriate fractions of all the phases and the overall material constitutive relations are a simple weighted average of the corresponding relations for the constituent phases.

(3) Stress-assisted martensitic transformation and slip/twinning are competing modes of plastic deformation in the transforming phase, while the matrix can undergo only slip/twinning.

(4) Both initial phases as well as martensite are elastically and plastically isotropic.

(5) Particles of the transforming phase do not interact with each other. They contain randomly oriented nucleation sites, and the activation of one of these nucleation sites causes complete transformation of the particle.

(6) Strain and stress partitioning is consistent with the Voigt upper bound model which postulates that the strains in all the phases are equal. This assumption may appear extreme and it was adopted only to make progress in this complex problem. It should be noted that Stringfellow *et al.* (1992) employed a more realistic self-consistent model.

(7) The evolution of martensite, as well as the evolution of the stresses, are assumed to be independent of the imposed strain rate.

Transforming dispersed phase. In order to completely describe the constitutive law for each of the constituent phases, the appropriate equations may be given which define: (a) the stress strain relationship; (b) the direction of plastic flow; (c) the yield criterion; and (d) the hardening rule. These equations are defined using the results of the analysis of transformation-controlled deformation discussed above.

The stress strain relationship. The stress strain relationship is defined here, within a hypoelastic basis which is appropriate for large strain rate-independent problems and the Kirchhoff stress $\mathbf{T}$, is chosen as a suitable measure of the stress state. The stress strain equation in the rate form is expressed as:

$$\overset{\nabla}{\mathbf{T}}_\beta = \boldsymbol{L}^e_\beta(\mathbf{D}_\beta - \mathbf{D}^p_\beta) \tag{34}$$

where the Jaumann derivative of the Kirchhoff stress, $\overset{\nabla}{\mathbf{T}}_\beta$, and the fourth order elasticity tensor, $\boldsymbol{L}^e_\beta$, in the transforming phase are, respectively, given as:

$$\overset{\nabla}{\mathbf{T}}_\beta = \dot{\mathbf{T}}_\beta - \mathbf{W}_\beta\mathbf{T}_\beta + \mathbf{T}_\beta\mathbf{W}_\beta \tag{35}$$

and

$$\boldsymbol{L}^e_\beta = 2G_\beta(\boldsymbol{I} - \tfrac{1}{3}\mathbf{I}\otimes\mathbf{I}) + B_\beta(\mathbf{I}\otimes\mathbf{I}). \tag{36}$$

$\dot{\mathbf{T}}_\beta$ is the material derivative of the Kirchhoff stress, $\mathbf{W}_\beta$ the spin tensor, $\boldsymbol{I}$ the fourth order identity tensor, $\mathbf{I}$ the second order identity tensor, G_β the elastic shear modulus and B_β, the elastic bulk modulus of the transforming phase. $\mathbf{D}_\beta$ and $\mathbf{D}^p_\beta$ in eqn (34) are the total stretching tensor and the plastic stretching tensor in the transforming phase, respectively.

The flow rule. The flow rule, which determines the direction of plastic flow for the transforming phase, is written in terms of the plastic stretching tensor as:

$$\mathbf{D}^p_\beta = \sqrt{\tfrac{3}{2}}\dot{\bar{\varepsilon}}_\beta\mathbf{N}_\beta + \dot{\varepsilon}_{h,\beta}\mathbf{I} \tag{37}$$

where $\mathbf{N}_\beta = \mathbf{T}'_\beta \,\|\, \mathbf{T}_\beta\beta\|$ is the deviatoric flow direction tensor. $\mathbf{T}'_\beta$, the deviatoric part of the Kirchhoff stress, $\dot{\bar{\varepsilon}}_\beta$ is the equivalent plastic strain rate, and $\dot{\varepsilon}_{h,\beta}$ is the dilatational plastic strain rate. The plastic strain increment for a given time increment Δt is now given by:

$$\Delta\varepsilon^p_\beta = \mathbf{D}^p_\beta\Delta t = \sqrt{\tfrac{3}{2}}\dot{\bar{\varepsilon}}_\beta\Delta t\mathbf{N} + \dot{\varepsilon}_{h,\beta}\Delta t\mathbf{I}. \tag{38}$$

At this point, it must be recognized that there may be two distinct contributions to the equivalent plastic strain rate, $\dot{\bar{\varepsilon}}_\beta$, in the transforming phase and they are: (a) $\dot{\bar{\varepsilon}}^{trans}$ associated with the martensitic transformation and (b) $\dot{\bar{\varepsilon}}^{slip}$ due to plastic deformation by slip/twinning. Using the incremental form of eqn (33), i.e., $\Delta\varepsilon^{trans}_{h,\beta} = \dot{\bar{\varepsilon}}^{trans}_{h,\beta}\,\Delta t = (\varepsilon_0/3)\,\Delta f$, and $\Delta\bar{\varepsilon}_\beta = \dot{\bar{\varepsilon}}_\beta\Delta t$, eqn (38) can be rewitten as:

$$\Delta\varepsilon^p_\beta = \sqrt{\tfrac{3}{2}}\Delta\bar{\varepsilon}_\beta\mathbf{N} + \frac{\varepsilon_0}{3}\Delta f\mathbf{I}. \tag{39}$$

The yield criterion. Based on eqn (22), a transformation yield criterion can be defined as:

$$\bar{\sigma}_\beta + k^*\sigma_{h,\beta} \leqslant R_\beta(\bar{\varepsilon}^{trans}_\beta) \tag{40}$$

where the yield resistance for the transforming phase as a function of the plastic strain, $R_\beta(\bar{\varepsilon}^{trans}_\beta)$ is obtained by substituting $f = \bar{\varepsilon}^{trans}_\beta/\varepsilon_1$ in eqn (22) in accordance with eqn (32). If

$\bar{\sigma}_\beta + k^* \sigma_{h,\beta} < R_\beta^{trans}$ in eqn (40), then the material is elastically deformed. Conversely, since $\bar{\sigma}_\beta + k^* \sigma_{h,\beta}$ cannot be greater than R_β^{trans}, as $\bar{\sigma}_\beta + k^* \sigma_{h,\beta}$ increases, transformation-induced plastic deformation causes an increase in the transformation resistance, R_β^{trans}, to accommodate higher stresses.

The plastic deformation by slip does not involve any volume change, and hence a pressure-independent yield criterion such as the Von Mises criterion can be used as:

$$\bar{\sigma}_\beta \leqslant R_\beta^{slip}(\bar{\varepsilon}_\beta^{slip}). \tag{41}$$

The slip yield resistance, R_β^{slip}, and its change with the equivalent slip plastic strain, $\bar{\varepsilon}_\beta^{slip}$, can, generally, be obtained by extrapolating the experimental uniaxial stress–strain data for the single (transforming) phase tested at high temperature at which the deformation is slip/twinning controlled down to lower temperatures at which transformation plasticity become important.

Since martensitic transformation and slip/twinning operate simultaneously, the overall yield resistance of the transforming phase can be defined as:

$$R_\beta(\bar{\varepsilon}_\beta) = \frac{1}{\dfrac{1}{R_\beta^{trans}(\bar{\varepsilon}_\beta)} + \dfrac{1}{R_\beta^{slip}(\bar{\varepsilon}_\beta)}}. \tag{42}$$

The hardening rule. The hardening rule specifies how the yield condition changes in the course of plastic deformation. It essentially defines the tangent modulus that governs plastic flow for the material, and is obtained by differentiating the yield resistance function with respect to the effective plastic strain as:

$$h_\beta = \frac{\mathrm{d}R_\beta(\bar{\varepsilon}_\beta)}{\mathrm{d}\bar{\varepsilon}_\beta} \tag{43}$$

where the beta phase yield functions R_β is given by eqn (42).

Nontransforming matrix phase

The stress strain relationship. The rate form of the stress–strain relationship is given by an equation analogous to eqn (34) except that the subscript γ for the nontransforming phase is used. The Jaumann derivative of the Kirchhoff stress, $\overset{\nabla}{\mathbf{T}}_\gamma$, and the fourth order elasticity tensor for the gamma phase, $\boldsymbol{L}_\gamma^e$, are given by the equations analogous to eqn (35) and (36), respectively.

The flow rule. Since the matrix phase undergoes a plastic deformation by slip or twinning but not by martensitic transformation, there is no accompanying volume change and hence the direction of the plastic flow should be set collinear with the deviatoric flow tensor $\mathbf{N}_\gamma = \mathbf{T}'_\gamma / \|\mathbf{T}'_\gamma\|$, and thus in accordance with eqn (38), the plastic strain increment can be defined as:

$$\Delta\varepsilon_\gamma^p = \mathbf{D}_\gamma^p \Delta t = \sqrt{\tfrac{3}{2}}\dot{\bar{\varepsilon}}_\gamma \Delta t \mathbf{N}_\gamma = \sqrt{\tfrac{3}{2}}\Delta\bar{\varepsilon}_\gamma \mathbf{N}_\gamma \tag{44}$$

where $\Delta\bar{\varepsilon}_\gamma$ is the equivalent plastic strain in the matrix phase.

The yield condition. Since the plastic flow in the gamma does not involve any volume change, a pressure independent yield condition such as the Von Mises yield criterion can be applied and an equation analogous to eqn (41) can be used.

The hardening rule. The rate of change in the yield resistance with the equivalent plastic strain can be defined by an equation analogous to eqn (42).

Two-phase material

The stress strain relationship. The relationship between the stress and the strain in rate form can be expressed as:

$$\overset{\nabla}{\mathbf{T}} = \boldsymbol{L}^e(\mathbf{D}-\mathbf{D}^p) \tag{45}$$

where $\overset{\nabla}{\mathbf{T}}$ and $\boldsymbol{L}^e$ are defined using a weighted average of the corresponding quantities for the two constituent phases. In addition, due to the use of the Voigt upper bound model, $\mathbf{D}^p = \mathbf{D}^p_\beta = \mathbf{D}^p_\gamma$.

The yield criterion. Based on eqns (40), (41) and the corresponding equation for the matrix phase, the yield criterion for the two-phase material can be written as:

$$\bar{\sigma} + f_\beta k^* \sigma_h \leqslant R(\bar{\varepsilon}) \tag{46}$$

where f_β is the volume fraction of the transforming phase.

The yield resistance for the two-phase material is defined by a weighted average of the corresponding yield resistance functions of the constituent phases, R_β and R_γ as:

$$R(\bar{\varepsilon}) = f_\beta R_\beta(\bar{\varepsilon}) + (1-f_\beta)R_\gamma(\bar{\varepsilon}). \tag{47}$$

The flow rule. Taking a weighted average of the expressions given by eqns (39) and (43), the increment in the plastic strain tensor in the two phase material can be written as:

$$\Delta\varepsilon^p = \mathbf{D}^p \Delta t = \sqrt{\frac{3}{2}}\Delta\bar{\varepsilon}\mathbf{N} + f_\beta \frac{\varepsilon_0 \Delta f}{3}\mathbf{I}. \tag{48}$$

The hardening rule. Since the yield criterion for the two-phase material has been defined as the weighted average of the yield functions for the two constituent phases, the hardening rule for the two-phase material is defined in the same manner. Thus:

$$h(\bar{\varepsilon}) = \frac{\mathrm{d}R(\bar{\varepsilon})}{\mathrm{d}\bar{\varepsilon}} = f_\beta h_\beta + (1-f_\beta)h_\gamma. \tag{49}$$

Determination of the material Jacobian

When a given boundary value problem is being solved using the finite element method, the knowledge of the material Jacobian for each Gaussian integration point at each time step is required to evaluate the elements stiffness matrix. Evaluation of the material Jacobian for the present constitutive model by a numerical integration of the material state is presented below.

If the Kirchhoff stress tensor at time t is $\mathbf{T}_0$, the updated stress tensor at a new time $t+\Delta t$ is then given by:

$$\mathbf{T} = \mathbf{T}_0 + \Delta\mathbf{T}. \tag{50}$$

The increment in stress $\Delta\mathbf{T}$ can be defined as the integral of the Jaumann stress rate tensor and is given by:

$$\Delta\mathbf{T} = \int_t^{t+\Delta t} \overset{\nabla}{\mathbf{T}}\,\mathrm{d}t. \tag{51}$$

Equation (51) can be evaluated numerically using the generalized trapezoidal rule as:

$$\Delta\mathbf{T} = \eta\overset{\nabla}{\mathbf{T}}\Delta t + (1-\eta)\overset{\nabla}{\mathbf{T}}_0\Delta t \quad (0 \leqslant \eta \leqslant 1). \tag{52}$$

In the present work, η was set to one, which reduces the trapezoidal rule to the Euler backwards difference method.

By combining eqns (50), (51) and (45), the updated stress tensor is now expressed as:

$$\mathbf{T} = \mathbf{T}_0 + \Delta t\boldsymbol{L}^e(\mathbf{D}) - \Delta t\boldsymbol{L}^e(\mathbf{D}^p). \tag{53}$$

To simplify the analysis, it was assumed here that the elastic properties of martensite are the same as those of the parent transforming phase. After introducing the total strain increment $\Delta\varepsilon$ as:

$$\Delta\varepsilon = \mathbf{D}\Delta t, \tag{54}$$

eqn (53) can be rewritten as:

$$\mathbf{T} = \mathbf{T}_0 + \boldsymbol{L}^e\Delta\varepsilon - \Delta t\boldsymbol{L}^e\mathbf{D}^p. \tag{55}$$

Since both the stress tensor from the previous time step, $\mathbf{T}_0$, and the total strain increment for the current time step, $\Delta\varepsilon$, are known, the first two terms on the right side of eqn (55) are known. The third term can be obtained by multiplying eqn (48) with $\boldsymbol{L}^e$.

Combining eqns (55), (36) and (48), and taking advantage of the fact that $\mathbf{N}$ is purely deviatoric, and hence $\mathbf{N}\cdot\mathbf{I} = 0$, yields:

$$\mathbf{T} = \mathbf{T}_0 + \boldsymbol{L}^e\Delta\varepsilon - \sqrt{6}G\bar{\dot{\varepsilon}}\Delta t\mathbf{N} - B\dot{f}_\beta\varepsilon_0 f\Delta t\mathbf{I}. \tag{56}$$

The $Bf_\beta\varepsilon_0\dot{f}\Delta t$ term represents a change in the hydrostatic stress due to the transformation volume change. This term is proportional to the equivalent transformation plastic strain increment, λ^{trans}, as follows:

$$Bf_\beta\varepsilon_0\dot{f}\Delta t = Bf_\beta\varepsilon_0\Delta f = Bf_\beta\varepsilon_0\frac{\mathrm{d}f}{\mathrm{d}\bar{\varepsilon}^{trans}}\lambda^{trans} = \frac{Bf_\beta\varepsilon_0}{\varepsilon_1}\lambda^{trans} = b\lambda^{trans} \tag{57}$$

where the proportionality constant, b, is defined as $b \equiv Bf_\beta\varepsilon_0/\varepsilon_1$, and $\mathrm{d}f/\mathrm{d}\bar{\varepsilon}$ is set to $1/\varepsilon_1$ in accordance with Fig. 7 and eqn (32). The transformation plastic strain increment λ^{trans} is assumed to be related to the total equivalent plastic strain increment $\lambda \equiv \bar{\dot{\varepsilon}}\Delta t$ as:

$$\lambda^{trans} = \frac{h_\beta^{slip}}{h_\beta^{slip} + h_\beta^{trans}}\lambda \tag{58}$$

where h_β^{slip} and h_β^{trans} are obtained by differentiating the R_β^{slip} and R_β^{trans} in accordance with eqns (22), (41) and (43). To simplify the computation, the $h_\beta^{slip}(h_\beta^{slip} + h_\beta^{trans})$ term in eqn (59) is assumed to be constant within a given time step and equal to its value at the beginning of the time step. Equation (56) can then be written as:

$$\mathbf{T} = \mathbf{T}_0 + \boldsymbol{L}^e\Delta\varepsilon - \sqrt{6}G\lambda\mathbf{N} - c\lambda\mathbf{I} \tag{59}$$

where c is a constant.

The Kirchhoff stress given by eqn (59) is next decomposed into its deviatoric component, $\mathbf{T}'$ and its hydrostatic component, $\frac{1}{3}tr(\mathbf{T})\mathbf{I}$ as:

$$\begin{aligned}\mathbf{T} &= \mathbf{T}' + \tfrac{1}{3}tr(\mathbf{T})\mathbf{I} \\ &= \mathbf{T}'_0 + 2G\Delta\varepsilon' - \sqrt{6}G\lambda\mathbf{N} + \tfrac{1}{3}tr(\mathbf{T}_0)\mathbf{I} + Btr(\Delta\varepsilon)\mathbf{I} - c\lambda\mathbf{I}.\end{aligned} \tag{60}$$

In accordance with eqn (46), the yield condition is given as a linear function of the deviatoric and hydrostatic stresses, as:

$$\sqrt{\frac{3}{2}}\| \mathbf{T}' \| + \frac{f_\beta k^*}{3} tr(\mathbf{T}) \leqslant R(\bar{\varepsilon}) = R(\bar{\varepsilon}_0 + \lambda) \tag{61}$$

where $R(\bar{\varepsilon})$ is the plastic flow resistance of the two phase material at the current level of the effective plastic strain, $\bar{\varepsilon} = \bar{\varepsilon}_0 + \lambda$.

To update the stress, the radial return procedure introduced by Kreig and Kreig (1977) is used. Towards that end, an elastic trial deviatoric stress, $\mathbf{T}'_T$.

$$\mathbf{T}'_I = \mathbf{T}'_0 + 2G\Delta\varepsilon' \tag{62}$$

and an elastic hydrostatic trial stress, $\frac{1}{3}tr(\mathbf{T}_T)\mathbf{T}$:

$$\tfrac{1}{3}tr(\mathbf{T}_T)\mathbf{I} = \tfrac{1}{3}tr(\mathbf{T}_0)\mathbf{I} + Btr(\Delta\varepsilon)\mathbf{I} \tag{63}$$

are defined.

In accordance with the method, the deviatoric stress is updated in the direction defined by $\mathbf{T}'_T$, and the magnitude of both hydrostatic and deviatoric trial stresses relaxed in accordance with eqn (60) as:

$$\|\mathbf{T}'\| = \|\mathbf{T}'_T\| = \sqrt{6}G\lambda \tag{64}$$

$$\tfrac{1}{3}tr(\mathbf{T}) = \tfrac{1}{3}tr(\mathbf{T}_T) - c\lambda \tag{65}$$

until the yield criterion given by the equality in eqn (61) is satisfied. By combining eqns (61), (64) and (65), the yield condition can be expressed as the following non-linear algebraic equation:

$$R(\bar{\varepsilon}_0 + \lambda) - \sqrt{\tfrac{3}{2}}[\|\mathbf{T}'_T\| - \sqrt{6}G\lambda] - f_\beta k^*[\tfrac{1}{3}tr(\mathbf{T}_T) - c\lambda] = 0. \tag{66}$$

This equation can be readily solved for the unknown increment in the equivalent plastic strain, λ. Furthermore substitution of eqns (62)–(65) into eqn (60), yields the following expression for the updated Kirchhoff stress:

$$\begin{aligned}\mathbf{T} &= [\|\mathbf{T}'\|]\mathbf{N} + [\tfrac{1}{3}tr(\mathbf{T})]\mathbf{I} \\ &= [\|\mathbf{T}'_0 + 2G\Delta\varepsilon\| - \sqrt{6}G\lambda]\mathbf{N} + [\tfrac{1}{3}tr(\mathbf{T}_0) + B\mathbf{tr}(\Delta\varepsilon) - c\lambda]\mathbf{I}.\end{aligned} \tag{67}$$

The updated stress tensor, $\mathbf{T}$, can hence be calculated by substituting the value for λ obtained as the solution of eqn (66) into eqn (67). The updated stress tensor is next used to determine the material Jacobian as described below.

The material Jacobian $\boldsymbol{J}$ is a fourth order tensor which represents the rate of change in the increment of the Kirchhoff stress, $\Delta\mathbf{T}$, with respect to a virtual change in the increment in strain, $\Delta\varepsilon$. Thus,

$$\boldsymbol{J} = \frac{\mathrm{d}\Delta\mathbf{T}}{\mathrm{d}\Delta\varepsilon}. \tag{68}$$

Using eqn (50) and the fact that $\mathbf{T}_0$ is a constant for the current time increment, the right hand side of eqn (68) can be written as follows:

$$\frac{d\Delta \mathbf{T}}{d\Delta\varepsilon} = \frac{d\mathbf{T}}{d\Delta\varepsilon} - \frac{d\mathbf{T}_0}{d\Delta\varepsilon} = \frac{d\mathbf{T}}{d\Delta\varepsilon}. \tag{69}$$

After substituting eqn (67) into eqn (69), the material Jacobian becomes,

$$\boldsymbol{J} = \frac{d}{d\Delta\varepsilon}[(\|\mathbf{T}'\|)\mathbf{N} + (\tfrac{1}{3}tr(\mathbf{T}_0) + Btr(\Delta\varepsilon) - c\lambda)\mathbf{I}]. \tag{70}$$

Each of the four terms in the brackets on the right hand side of eqn (70) are next differentiated, and expressed using the appropriate equations of the current material constitutive model, and combined to give a sum of five independent fourth order tensors as:

$$\boldsymbol{J} = C_1\boldsymbol{I} + C_2\mathbf{I}\otimes\mathbf{I} + C_3\mathbf{N}\otimes\mathbf{N} + C_4\mathbf{N}\otimes\mathbf{I} + C_5\mathbf{I}\otimes\mathbf{N} \tag{71}$$

where:

$$C_1 = 2G\frac{\|\mathbf{T}'\|}{\|\mathbf{T}'_T\|} \tag{72}$$

$$C_2 = B - \frac{f_\beta k^* Bc}{h + f_\beta k^* c + 3G} - \frac{2G}{3}\frac{\|\mathbf{T}'\|}{\|\mathbf{T}'_T\|} \tag{73}$$

$$C_3 = 2G\frac{h + f_\beta k^* c}{h + f_\beta k^* c + 3G} - 2G\frac{\|\mathbf{T}'\|}{\|\mathbf{T}'_T\|} \tag{74}$$

$$C_4 = -\frac{\sqrt{6}Gf_\beta k^* B}{h + f_\beta k^* c + 3G} \tag{75}$$

$$C_5 = -\frac{\sqrt{6}Gc}{h + f_\beta k^* c + 3G}. \tag{76}$$

A detailed derivation of eqns (71)–(76) is given by Sankaran (1996).

ANALYSIS OF UNIAXIAL TENSILE DUCTILITY OF THE GAMMA TiAl/BETA Ti-Al-V-Fe PHASE SYSTEM

Determination of the yield resistances and failure criterion

The materials constitutive relations developed in the previous section are next used to analyze uniaxial tensile behavior of the material system consisting of a gamma TiAl matrix and dispersed particles of a Ti-Al-V-Fe transforming beta phase.

The yield resistance curve for gamma TiAl has been determined by fitting the experimental room-temperature uniaxial stress–strain data of Krishnamurthy and Kim (1991) to a function:

$$R_\gamma = K_\gamma(\bar{\varepsilon}_\gamma)^{n_\gamma}. \tag{77}$$

This procedure yielded $K_\gamma = 895.8$ MPa and $n_\gamma = 0.128$.

In a similar fashion, the slip resistance for the beta phase was determined by fitting the high temperature uniaxial stress–strain data of Duerig *et al.* (1980) to a function:

$$R_\beta^{slip} = K_\beta(\bar{\varepsilon}_\beta^{slip})^{n_\gamma} \tag{78}$$

and extrapolating the K_β vs T and n_β vs T functions to room temperature. This procedure yielded $K_\beta = 1385$ MPa and $n_\beta = 0.145$.

To completely define the transformation yield resistance function for the beta phase, eqn (22), the room-temperature martensitic transformation Gibbs free energy change, $\Delta g^{\gamma h}$, for a given chemical composition of the beta phase was calculated using the thermodynamic procedure developed by Grujicic (1992). All other parameters appearing in eqn (22), such as $\beta = 2.73$, $\gamma_0 = 0.08$, etc. were set to the value given in the previous section since these values are typical for the Ti-Al-V-Fe beta phase.

To complete the description of the two phase gamma TiAl/beta Ti-Al-V-Fe phase system, the volume fraction of the beta phase f_β was set to 0.1 and the following elastic properties were assigned to the two phases: $G_\gamma = 6.15$ GPa, $B_\gamma = 133.3$ GPa, $G_\beta = 26.9$ GPa and $B_\beta = 58.3$ GPa.

Next, a fracture criterion controlling the tensile ductility is selected. Following the suggestion of Chan (1992), a stress-controlled fracture criterion is adopted which is consistent with the fact that tensile ductility in the present material system is controlled by the nucleation of microcracks that are, at initiation, longer than the length required to attain the critical value of the stress intensity factor K_{IC}. Following the analysis of Thomson and Hancock (1984), which showed that the microcrack nucleation process is influenced by both the equivalent stress, $\bar{\sigma}$, and the hydrostatic stress, σ_h, the following failure function, which combines these two stress invariants is used:

$$g(\bar{\sigma}(\bar{\varepsilon}), \sigma_h(\bar{\varepsilon})) = \sqrt{\left[\frac{\bar{\sigma}(\bar{\varepsilon})}{\bar{\sigma}_f}\right]^2 + \left[\frac{\sigma_h(\bar{\varepsilon})}{\sigma_{h,f}}\right]^2} \tag{79}$$

where $\bar{\sigma}_f$ is the equivalent stress required for fracture in the absence of any hydrostatic stress, and $\sigma_{h,f}$ is the hydrostatic stress required for fracture in the absence of any equivalent stress. The term σ_h, which is, in general, a function of the dilatational strain, ε_h, becomes, in the case of transformation controlled plasticity, a function of the equivalent strain since according to eqns (32) and (33), $\varepsilon_h = (\varepsilon_0/3\varepsilon_1)\bar{\varepsilon}$. The failure function, at a material point, can take on a value between 0.0 to 1.0 with $g = 0.0$ corresponding to the stress free condition, and $g = 1.0$ is associated with the moment of fracture. The material constants $\bar{\sigma}_f$ and $\sigma_{h,f}$, appearing in eqn (79), are evaluated using the following procedure: First, the $\bar{\sigma}_f/\sigma_{h,f}$ ratio is assumed to be equal to the ratio of the theoretical shear strength and the theoretical strength of the material. As shown by Dieter (1988), the latter ratio is equal to $2E/G$, where E and G, respectively, the Young's modulus and the shear modulus of the two-phase material. The second relationship between $\bar{\sigma}_f$ and $\sigma_{h,f}$ is obtained by setting failure function, g, in eqn (79) equal to 1.0 at the uniaxial fracture stress of the single phase gamma TiAl uniaxial fracture stress, $\sigma = 498$ MPa, as reported by Chan (1992) and then substituting $\bar{\sigma} = \sigma/3$ and $\sigma_h = \sigma/3$ in eqn (79). This procedure yielded the pure shear fracture strength $\bar{\sigma}_f = 255$ MPa while the pure hydrostatic fracture strength $\sigma_{h,f} = 1323$ MPa.

Simulation of a tensile test

We next proceed with the simulation of a uniaxial tensile test for a smooth bar (a bar with the uniform cross sectional area), using the finite element program ABAQUS, in order to analyze the effect of dispersed particles of the transforming beta phase on the uniaxial stress–strain behavior of the gamma Ti-Al based material and, in particular, on tensile ductility (the uniaxial plastic strain at fracture). This is done using one 4 noded isoparametric quadrilateral axisymmetric element under displacement control loading boundary conditions. It should be noted that the simulation of a tensile bar that retains a uniform cross sectional area can be done by a simple integration of the materials constitutive relation and a finite element approach is not necessary. However, since the smooth-bar tensile test was only one of the simulations we performed, and the others including the tensile test of a notched bar and a crack propagation problem required the use of the finite element method, Sankaran (1996), the smooth-bar tensile test simulation was carried out using the finite element approach.

The effect of thermodynamic stability of the transforming beta phase on the tensile ductility, for a gamma TiAl based alloy containing 10 volume percent of the beta phase

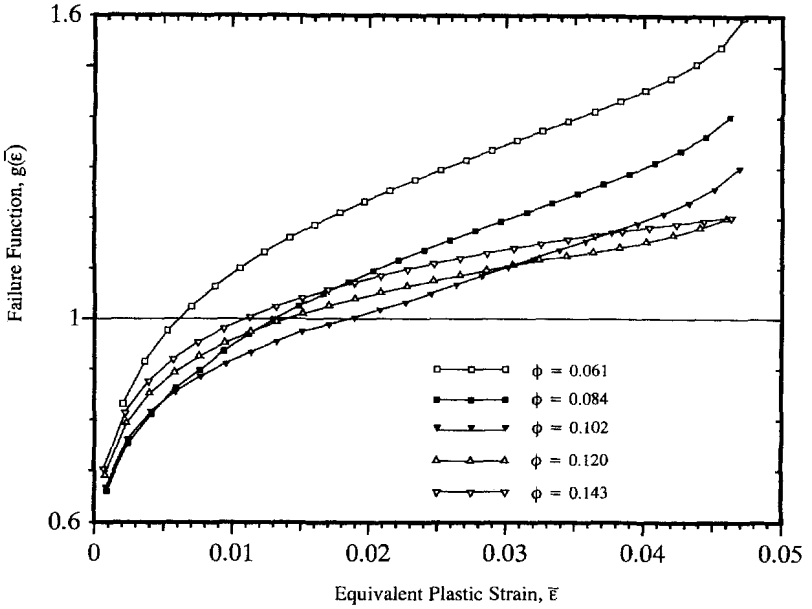

Fig. 11. Effect of the thermodynamic stability of the dispersed beta phase on the failure function for a 10% dispersion of beta phase in a gamma TiAl matrix.

dispersion is investigated for nine different levels of the normalized chemical driving force in the range between $\phi = 0.06$ and $\phi = 0.145$. The evolution of the failure function with equivalent plastic strain for five of the nine levels of thermodynamic stability is shown in Fig. 11. The observed downward shift in the failure function vs. plastic strain curve with an increase in the chemical driving force in the range between $\phi = 0.06$ and $\phi = 0.102$ can be attributed to the fact that as the thermodynamic stability of the beta phase is lowered, the magnitude of the stress required to achieve the same level of total (chemical + mechanical) driving force is reduced. However, as the thermodynamic stability of the beta phase decreases, the extent of thermally activated martensitic transformation prior to loading also increases. This results in a lower effective volume fraction of the metastable phase being available for transformation during loading. In the limit of very low thermodynamic stability, practically all the beta phase particles will be thermally transformed. In all the simulation runs, the effective volume fraction of the metastable beta phase is determined by subtracting the thermally-transformed fraction from the total volume fraction of this phase.

The results shown in Fig. 11 suggest that there exists an optimum value of the chemical driving force with respect to achieving a maximum in tensile ductility. This is more clearly seen in Fig. 12 in which the uniaxial fracture strain (strain corresponding to the condition $g = 1.0$) is plotted against the normalized chemical driving force, ϕ. The results displayed in Fig. 12 show that the optimum thermodynamic stability of the transforming beta phase corresponds to a normalized chemical driving force level of approximately 0.102, and the associated maximum level of tensile ductility corresponds to the plastic fracture strain of ~ 0.0186. For comparison, the plastic fracture strain in the pure gamma TiAl described by eqns (77) and (79) is ~ 0.09.

In a comprehensive study involving design of the beta phase for dispersed phase transformation toughening of gamma TiAl, Grujicic and Narayan (1992) identified the Ti-30Al-65V-2-7Fe (wt%) chemical composition range of the beta phase as that which meets the necessary requirements regarding the positive character of the transformation volume change and the gamma/beta high-temperature chemical compatibility. In addition, using a very simple thermodynamics/mechanics analysis of stress-assisted martensitic transformation, Grujicic and Narayan (1992) determined that 5 wt% Fe gives rise to the optimum level of thermodynamic stability of the beta phase. Grujicic and Dang (1996) then demonstrated that the addition of 10 volume percent of the Ti-30Al-65Fe-5Fe (wt%) beta phase into the gamma TiAl intermetallic nearly doubles the tensile ductility. The

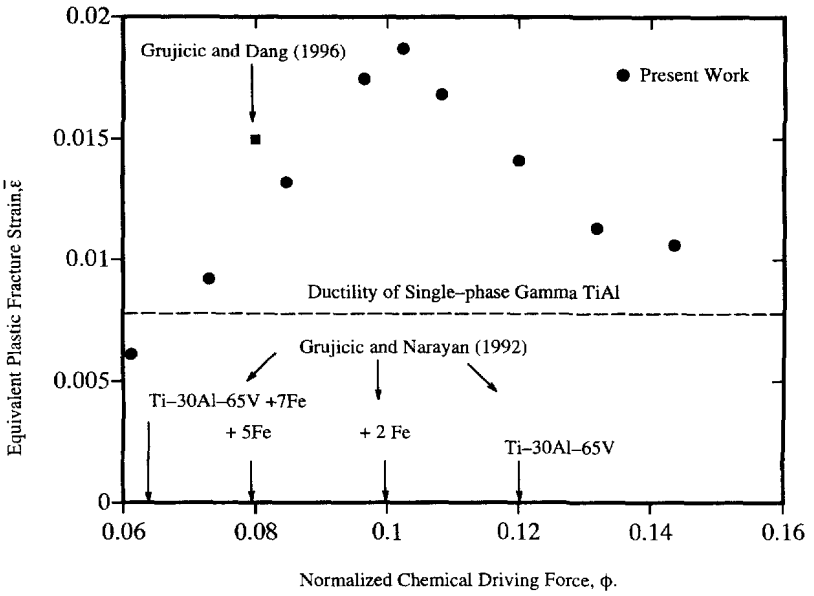

Fig. 12. Effect of the thermodynamic stability of the dispersed beta phase on tensile ductility for a 10% dispersion of beta phase in a gamma TiAl matrix.

normalized chemical driving force and the predicted levels of tensile ductility for the four beta alloys containing 0, 2, 5 and 7 wt% of iron analyzed by Grujicic and Narayan (1992) are indicated in Fig. 12. Also shown in Fig. 12, are the tensile ductility levels in pure gamma TiAl and in the two phase gamma/beta alloy analyzed by Grujicic and Dang (1996). The 2 wt% Fe content in the Ti-30Al-65V (wt%) beta phase appears to be associated with thermodynamic driving force closest to the optimum one.

A comparison of the computed levels of tensile ductility and the experimental data of Grujicic and Dang (1996) shows that the proposed model accounts for about 50% of the transformation-enhanced ductility effect in the gamma TiAl alloy containing 10 vol.% of the Ti-30Al-65V-5Fe (wt%) beta phase. While this is a reasonable agreement, it must be recognized that few important phenomena such as the interaction between the beta phase particles, which enhance the rate of transformation, generation of the additional potent nucleation sites due to slip, etc., are not taken into account by the model. No attempt was made to assess the contribution of these phenomena.

ANALYSIS OF UNIAXIAL TENSILE BEHAVIOR OF THE BETA/ALPHA Ti-10V-2Fe-3Al SYSTEM

Because of its limited ductility, the gamma TiAl/beta phase material system analyzed in the previous section does not allow us to test the ability of the present model to account for material behavior at larger strains. To carry out such a test, the behavior of a two-phase beta/alpha Ti-10V-2Fe-3Al (wt%) alloy system, studied experimentally by Duerig *et al.* (1980), was simulated using a finite element procedure analogous to that described in the previous section. The yield resistance curve for the alpha phase, was determined by fitting the experimental uniaxial stress–strain data of Conrad and Jones (1970) to a power law function analogous to eqn (77). This yielded $K_\alpha = 1076$ MPa and $n_\alpha = 0.135$.

To determine the transformation yield resistance for the beta phase, eqn (22), the procedure of Grujicic (1992) was used to first calculate the chemical composition of the beta phase in equilibrium with the alpha phase and next to compute the chemical Gibbs free energy change, Δg^{ch}. To complete the description of the two-phase beta/alpha system, the volume fraction of the alpha phase $f_\alpha = 1 - f_\beta$ is set to 0.1 and the elastic properties $G_\alpha = 58$ GPa, $B_\alpha = 126$ GPa, assigned to this phase.

It should be pointed out that while the two phase alloy analyzed here contained 90 vol.% of the beta phase, the alpha phase is distributed mostly as a continuous film along

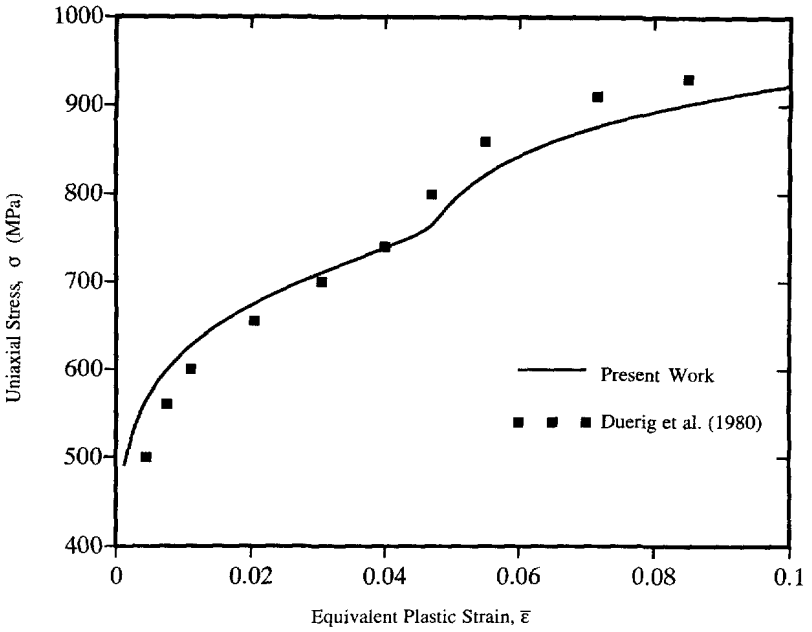

Fig. 13. Uniaxial stress strain behavior of two-phase beta-phase based Ti-10V-2Fe-3Al alloy containing a 10 vol.% of the alpha phase dispersion.

the beta-phase grain boundaries and hence the assumption regarding the discrete nature of the beta phase particles (grains) appear to be justified.

The results of the simulation and the corresponding experimental results of Duerig *et al.* (1980) are shown in Fig. 13. A reasonable agreement between the predicted and measured sigmoidal stress–strain curves is obtained over the entire plastic strain range of the alloy. This finding suggests that the material constitutive model developed in the present work captures the main features of the transformation-controlled plastic deformation in dispersed phase materials systems.

In closing, one may argue that the same agreement between the experimental and the predicted stress–strain curves could be achieved with fewer parameters. While this is true, the present formulation of the materials constitutive relations, which accounts for the basic statistics and thermodynamic aspects of the martensitic transformation is portable to other alloy systems undergoing a dispersed-phase stress-assisted martensitic transformation.

Acknowledgements—The work has been supported by the National Science Foundation under Grants DMR-9317804 and CMS-9531930. The authors are indebted to Drs Bruce A. MacDonald and William A. Spitzig of NSF for his continuing interest in the present work. We are also thankful to Professor S. Ahzi for his assistance on the analysis of martensitic transformation under stress. The stimulating discussion carried out with Professor D. M. Parks of MIT and Dr G. B. Olson of Northwestern University are appreciated.

REFERENCES

Budiansky, B., Hutchinson, J. W. and Lambropoulos, J. C. (1983) Continuum theory of dilatant transformation toughening in ceramics. *International Journal of Solids and Structures* **19,** 337–355.

Cech, R. E. and Turnbull, D. (1956) Heterogeneous nucleation of the martensite transformation. *Transactions AIME* **206,** 124–132.

Chan, K. S. (1992) Understanding fracture in gamma TiAl. *JOM* **44,** 30–38.

Chen, I.-W., Chiao, Y.-H. and Tsuzaki, K. (1985) Statistics of martensitic nucleation. *Acta Metallica* **33,** 1847–1859.

Conrad H. and Jones R. (1970) Effects of interstitial content and grain size on the mechanical behavior of alpha titanium below 0.4Tm. In *The Science, Technology and Application of Titanium*, eds R. I. Jaffee and N. E. Promisel. Pergamon Press, Oxford, pp. 81–501.

Dieter, G. E. (1988) *Mechanical Metallurgy*. McGraw-Hill Book Co., Maidenhead, pp. 243–245.

Duerig, T. W., Terlinde, G. T. and Williams, J. C. (1980) Phase transformations and tensile properties of Ti-10V-2Fe-3Al. *Metal Transactions A* **11A,** 1987–1998.

Evans, A. G. and Cannon, R. M. (1986) Toughening of brittle solids by martensitic transformations. *Acta Metallica* **34,** 761–800.

Grujicic, M. (1992) Design of Ti-Al-V beta phase for transformation toughening of gamma TiAl. *Materials Science Engineering* **A151,** 75–78.

Grujicic, M. and Dang, P. (1996) Martensitic transformation in a dispersed phase Ti-Al-V-Fe phase and its effect on fracture toughness of gamma titanium aluminide. *Material Science Engineering* (submitted).

Grujicic, M. and Narayan, C. P. (1992) A study of beta to alpha double prime martensitic transformation volume change in Ti-Al-V alloys. *Material Science Engineering* **A15,** 217–226.

Hom, C. L. and McMeeking, R. M. (1990) Numerical results for transformation toughening in ceramics. *International Journal of Solids and Structures* **26,** 1211–1223.

Kreig, R. D. and Kreig, D. B. (1977) Accuracies of numerical solution methods for the elastic-perfectly plastic model. *Journal of Pressure Vessel Technology, ASME* **99,** 510–518.

Krishnamurthy, S. and Kim, Y.-W. (1991) The temperature dependence of tensile behavior of a gamma titanium aluminide alloy. In *Microstructure/property Relationships in Titanium Aluminides and Alloys*, pp. 149–163.

Olson, G. B. (1987) Overview: Science of steel. In *Innovations in Ultra-high Strength Steel Technology*, eds G. B. Olson, M. Azrin and E. S. Wright. Sagamore Army materials research conference proceedings, pp. 3–66.

Olson, G. B. Tsuzaki, K. and Cohen, M. (1987) Statistical aspects of martensitic nucleation. *Material Research Symposium Proceedings* **57,** 129–148.

Patel, J. and Cohen, M. (1953) Criterion for the action of applied stress in the martensitic transformation. *Acta Metallica* **1,** 531–538.

Sankaran, N. (1996) Continuum analysis of transformation-enhanced ductility and toughness in gamma TiAl/beta Ti-Al-V-Fe phase system. MS thesis, Clemson University, U.S.A.

Stringfellow, R. G., Parks, D. M. and Olson, G. B. (1992) A constitutive model for transformation plasticity accompanying strain-induced martensitic transformations in metastable austenitic steels. *Acta Metallica Materiala* **40,** 1703–1716.

Thomson, R. D. and Hancock, J. W. (1984) Ductile failure by void nucleation, growth and coalescence. *International Journal of Fracture* **26,** 99–112.